

Nearly room temperature ferromagnetism in pressure-induced correlated metallic state of van der Waals insulator CrGeTe₃

Dilip Bhoi,^{1,*} Jun Gouchi,¹ Naoka Hiraoka,² Yufeng Zhang,^{1,3} Norio Ogita,⁴ Takumi Hasegawa,⁴ Kentaro Kitagawa,² Hidenori Takagi,^{2,5,6} Kee Hoon Kim,^{7,8} and Yoshiya Uwatoko¹

¹*The Institute for Solid State Physics, University of Tokyo, Kashiwa, Chiba 277-8581, Japan*

²*Department of Physics, Graduate School of Sciences, University of Tokyo, Tokyo 113-0033, Japan*

³*School of Physics, Southeast University, Nanjing 211189, China*

⁴*Graduate School of Integrated Arts and Sciences,*

Hiroshima University, Higashi-Hiroshima, Hiroshima 739-8521, Japan

⁵*Institute for Functional Matter and Quantum Technologies,*

University of Stuttgart, 70569 Stuttgart, Germany

⁶*Max Planck Institute for Solid State Research, Heisenbergstraße 1, 70569 Stuttgart, Germany*

⁷*Department of Physics and Astronomy, CeNSCMR,*

Seoul National University, Seoul, 151-747, Republic of Korea

⁸*Institute of Applied Physics, Seoul National University, Seoul, 151-747, Republic of Korea*

(Dated: July 23, 2021)

A complex interplay of different energy scales involving Coulomb repulsion, spin-orbit coupling and Hund's coupling energy in two-dimensional (2D) van der Waals (vdW) material produces novel emerging physical state. For instance, ferromagnetism in vdW charge transfer insulator CrGeTe₃, that provides a promising platform to simultaneously manipulate the magnetic and electrical properties for potential device implementation using few layers thick materials. Here, we show a continuous tuning of magnetic and electrical properties of CrGeTe₃ single crystal using pressure. With application of pressure, CrGeTe₃ transforms from a FM insulator with Curie temperature, $T_C \sim 66$ K at ambient condition to a correlated 2D Fermi metal with T_C exceeding ~ 250 K. Notably, absence of an accompanying structural distortion across the insulator-metal transition (IMT) suggests that the pressure induced modification of electronic ground states are driven by electronic correlation furnishing a rare example of bandwidth-controlled IMT in a vdW material.

Discovery of two-dimensional (2D) magnetism in van der Waals (vdW) materials have unfurled diverse range of possibilities for development of novel spintronics, multiferroic and quantum computing devices using atomically thin material as well as fundamental research [1–6]. These also include exploration of exotic physics such as Kitaev quantum spin liquid state in 3d electron system with $S = 3/2$ [7, 8]. Until now, CrYTe₃ ($Y = \text{Ge, Si}$) [9, 10], CrX₃ ($X = \text{I and Br}$) [11–15], 1T-CrTe₂ [16, 17] and Fe_{3-x}GeTe₂ [18–21], are the few vdW materials known to exhibit ferromagnetic (FM) order in bulk single crystal form and retain intrinsic ferromagnetism down to monolayer limit. Among these, CrYTe₃ and CrX₃ are Mott insulators with a charge gap, facilitating a suitable platform to exploit both charge and spin degrees of freedom.

At low temperature, these Cr-based vdW insulators share a common layered rhombohedral $R\bar{3}$ crystal structure held together by weak vdW forces along the c -axis [10–12]. Each single layer consists of a honeycomb network of edge sharing octahedra formed by a central Cr atom bonded to six ligand atoms (Te or X), as illustrated in Fig.1(a) for CrGeTe₃ as a representative. Crystalline field effect ensuing from this octahedra splits Cr-3d orbitals into t_{2g} - and e_g -manifolds [Fig.1(b)]. The onsite Coulomb repulsion localizes the t_{2g} -electrons driving the system into an insulating state significantly well above the Curie temperature, T_C [22–24]. Although, a direct

antiferromagnetic (AFM) exchange interaction exists between t_{2g} electrons, thermal fluctuation inherent to 2D suppress the long-range magnetic order. The spin orbit coupling (SOC) emanating through the covalent bond between ligand p and Cr- e_g orbital generates the magnetocrystalline anisotropy energy (MAE) to counteract the thermal fluctuation [24, 25]. Below T_C , superexchange interaction between the active Cr- e_g electrons via two different ligand p -orbitals, as schematically portrayed in Fig.1(c), benefits from distortion of CrTe₆ octahedra and Hund's energy gain at the ligand Te (or X) site to stabilize the FM order [22, 24, 26]. Moreover, correlation between t_{2g} -electrons also move up the ligand p bands close to Fermi level, thus opening a band gap between Cr d conduction band and ligand p valence band confirming the charge transfer type Mott behaviour [22–24, 26, 27].

The charge gap of a Mott insulator can be manipulated either by carrier doping which fills the band or by controlling the bandwidth, resulting in an insulator-metal transition (IMT) often accompanied by a structural and magnetic transitions. So far, doping through gating a field effect transistor (FET) device [28–30], or intercalation of organic ions to bulk single crystals [31] have been used. With electrostatic gating to few layers of CrGeTe₃ [28] and CrI₃ [29], the coercive field and saturation magnetization are found to be modulated, but T_C changes barely. However, when high carrier density ($\sim 10^{-14}$ cm⁻²) is doped to CrGeTe₃ either through intercalation

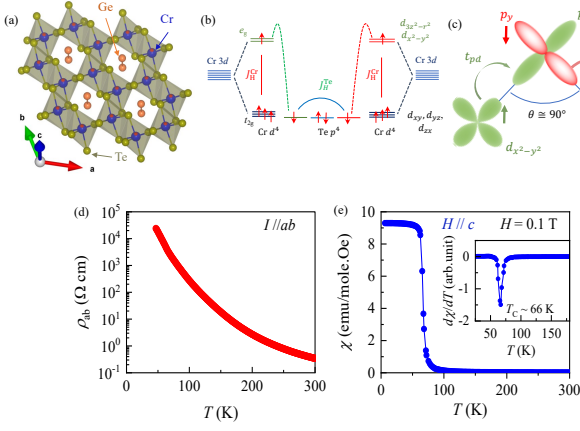


FIG. 1. (a) Single layer of CrGeTe₃ illustrating the honeycomb network of edge sharing CrTe₆ octahedra. In case of CrX₃, the place of Ge-Ge dimers remains vacant. (b) Crystalline electric field splitting of Cr 3d orbitals into t_{2g} - and e_g -manifolds. (c) Schematic picture of indirect superexchange FM interaction between Cr e_g -orbitals via two Te p -orbitals, where J_H^{Cr} and J_H^{Te} are respectively the Hund's coupling at Cr and Te site. $t_{pd}(t_{p'd'})$ is the virtual hopping between $e_g(e'_g)$ and $p(p')$ orbitals. (d) Temperature dependence of the in-plane resistivity, ρ_{ab} , with current flowing in the ab -plane. (e) Zero field-cooled (ZFC) dc magnetic susceptibility, χ , measured at field $H = 0.1$ T applied along the easy magnetization c -axis. Inset shows the temperature derivative, $d\chi/dT$.

[31] or ionic liquid gating to FET devices [30], T_C around ~ 200 K is achieved with simultaneous stabilization of a metallic state. Although these results are promising, nevertheless, such filling controlled methods lead to undesirable effects such as strong charge in-homogeneity in atomic scale either due to disorder created by intercalant ions or chemical modification of the host material induced by ionic liquid [32].

On the contrary, application of pressure is an alternative route, which not only controls the bandwidth but also the spin exchange pathways via subtle modification of bond length and angle between atoms avoiding the complication of disorder. Pressure has been suitably used to switch the interlayer magnetism of few layers of CrI₃ [33, 34] including T_C variation of CrI₃ and CrGeTe₃ bulk single crystals [35–37]. However, these studies are limited to less than 2.0 GPa with T_C varying about $\sim 10\%$. Interestingly, a recent high pressure work on CrSiTe₃ [38] revealed a concomitant structural transition and IMT followed by a superconductivity around 7.0 GPa.

In this work, we study the electronic and magnetic properties of CrGeTe₃ single crystals by varying pressure up to 11.0 GPa using dc magnetic susceptibility and resistivity measurement. Although, the pressure dependent lattice dynamics of CrGeTe₃ have been performed revealing a 2D to 3D structural transition around ≥ 18 GPa [35, 39], the magnetic and electrical properties at high pressure have remain unexplored. At ambient pres-

sure, CrGeTe₃ is an insulator with a band gap of ~ 0.7 eV [40] and orders in a Heisenberg type ferromagnetism below $T_C \sim 66$ K as shown in Fig.1(d,e). At first, T_C decreases monotonically to 54 K as pressure increases to 4.5 GPa. Remarkably, T_C jumps four-fold in between $4.5 \leq P \leq 7.5$ GPa and surpasses 250 K above 9.1 GPa. The pressure temperature phase diagram uncovers an IMT to a correlated Fermi metallic state above ~ 7.0 GPa, characterized by large resistivity anisotropy, $\rho_c/\rho_{ab} \sim 10^5$, suggesting 2D nature of charge transport. Our results suggest collapse of charge transfer energy gap between Te- p valence band and Cr- e_g conduction band dramatically boost the intra-layer FM superexchange interaction producing such a high T_C . In addition, these results provide a rare example of bandwidth-controlled IMT in a vdW material, without entailing simultaneous structural transition and spin-crossover from magnetic to non-magnetic state.

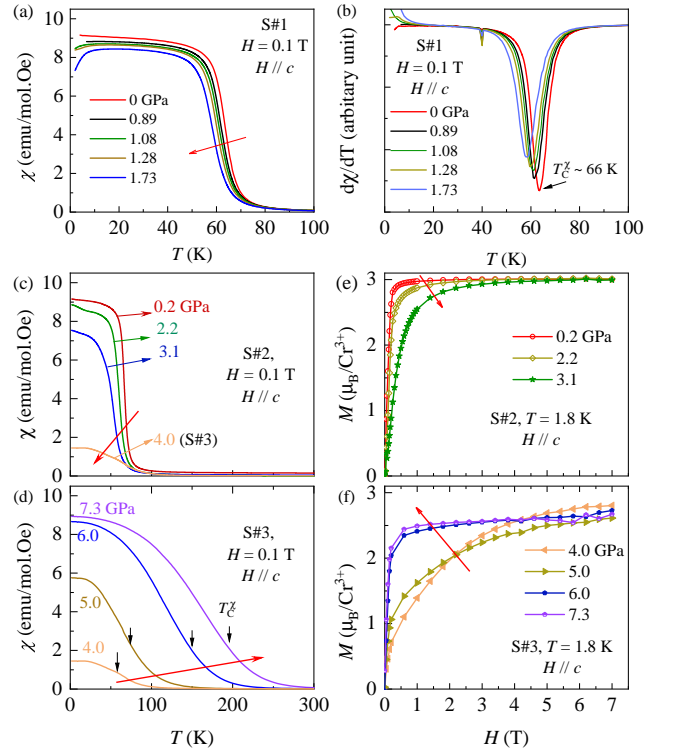


FIG. 2. (a) Temperature dependence of ZFC dc susceptibility, χ of CrGeTe₃ crystal S#1 at $H = 0.1$ T applied parallel to c -axis for pressure up to 1.73 GPa. (b) Temperature dependence of $d\chi/dT$ of S#1. The temperature dependence of field-cooled (FC) susceptibility, χ , for (c) crystal S#2 and (d) crystal S#3, respectively. The field dependence of magnetization, $M(H)$, for (e) S#2 and (f) S#3 at $T = 1.8$ K under different pressure. Red arrows in figures represent the direction of increasing pressure.

In Fig.2(a), we illustrate the temperature dependence of dc susceptibility, χ , of CrGeTe₃ single crystal (S#1) with an applied magnetic field $H = 0.1$ T parallel to

c -axis at several pressure. At ambient pressure, $\chi(T)$ undergoes a typical paramagnet to FM transition and the estimated $T_C^\chi \sim 66$ K, from the minimum of $d\chi/dT$ curve is consistent with several earlier reports [40–42]. With increasing pressure up to 1.73 GPa (Fig.2(a)), the transition shifts towards lower temperature and T_C^χ reduces to ~ 58 K at 1.73 GPa [see Fig.2(b)]. The weak downturn of χ below ~ 7.0 K at 1.08 GPa is related to the formation of FM domains in the crystal as evidenced by the bifurcation between FC and ZFC curve [see supplementary Fig.S2]. To track further the evolution of T_C above 2.0 GPa, we measured χ of another two pieces of CrGeTe₃ single crystals extracted from the same batch using an opposed-anvil type pressure cell [43]. Fig.2(c) and (d) present the temperature dependence of χ for crystals S#2 and S#3, respectively. Although the magnitude of χ decreases drastically as pressure is raised to 4.0 GPa [Fig.2(c)], T_C^χ decreases modestly to ~ 54 K. Surprisingly, as pressure is increased further the magnitude of χ surges again and transition shifts towards higher temperature [Fig.2(d)]. For $P \geq 5.0$ GPa, $\chi(T)$ curves show a broad transition to a FM state with $T_C^\chi \sim 73$ K. At 7.3 GPa, T_C^χ reaches as high as ~ 196 K, almost three times higher than the T_C^χ at ambient pressure.

In Fig.2(e) and (f), we present the $M(H)$ curve along the easy magnetization c -axis for crystals S#2 and S#3, respectively. At 0.2 GPa, $M(H)$ curve saturates sharply at $H_S \cong 0.22$ T with a saturation moment $M_S \sim 3.0\mu_B/\text{Cr}^{3+}$. With variation of pressure $M(H)$ curve becomes rounder and H_S surpasses 3.0 T at 3.1 GPa. At 4.0 GPa, $M(H)$ curve look similar to a Brillouin like function and does not saturate even up to 7.0 T. Even though, $M(H)$ curve resembles typically observed in a paramagnet, the Curie-Weiss temperature, θ_{CW} , at this pressure is comparable with that of ambient condition, hinting the presence of strong FM interaction (see supplementary Fig.S3). For $P \geq 5.0$ GPa, H_S start to decrease again. At $P \cong 6.0$ GPa, $M(H)$ curve saturate sharply above $H_S \cong 0.18$ T with $M_S \sim 2.76 \mu_B/\text{Cr}^{3+}$, a typical sign of FM order. From the evolution of $\chi(T)$ and $M(H)$ curves under pressure, it is clear that in the intermediate pressure range $3.1 \text{ GPa} \leq P \leq 5.0 \text{ GPa}$, the net FM exchange interaction weakens, producing a diminished $\chi(T)$ magnitude and T_C^χ .

Next, we show the temperature dependence of in-plane resistivity, ρ_{ab} , of CrGeTe₃ under pressure ranging from 0 to 11 GPa, in Fig.3(a), revealing an insulator to metal transition (IMT). The overall ρ_{ab} plummet several orders of magnitude as 11.0 GPa pressure is applied; at low temperature ρ_{ab} falls more than nine orders of magnitude, while at $T = 300$ K more than three orders. At 2.0 GPa, $\rho_{ab}(T)$ discloses a shoulder-like anomaly at $T_C^\rho \sim 59$ K, very close to the FM transition observed in $\chi(T)$, allowing to trace the evolution of magnetic order with pressure from ρ_{ab} data. T_C^ρ falls to ~ 54 K at 4.5 GPa. However, at 5.0 GPa, ρ_{ab} exhibits a broad maximum at ~ 73 K

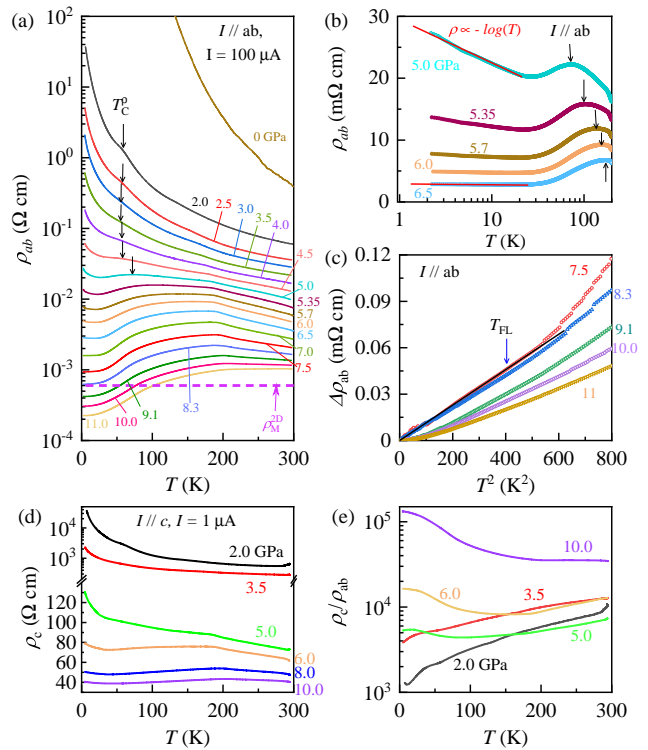


FIG. 3. (a) Temperature dependence of in-plane resistivity, ρ_{ab} , of a CrGeTe₃ single crystal at several pressure ranging from 0 to 11.0 GPa, disclosing an insulator to metal transition. The horizontal magenta dotted line represents an estimate of the Mott-Ioffe-Regel limit of resistivity, ρ_M^{2D} , as described in the text. (b) Temperature dependence of ρ_{ab} in logarithmic temperature scale. Red solid lines are $-\log(T)$ fit to ρ_{ab} . Black downward arrows trace T_C^ρ with pressure. (c) $\Delta\rho_{ab} = (\rho_{ab} - \rho_0)$ vs T^2 for $P \geq 7.5$ GPa, where ρ_0 is the residual resistivity. The black line is a linear fit to $\Delta\rho$ at 7.5 GPa confirming a Fermi liquid state below T_{FL} . (d) The out-of-plane resistivity, ρ_c , at some selected pressure. (e) Temperature dependence of resistivity anisotropy, ρ_c/ρ_{ab} , at different pressure.

[Fig.3(b)], an indication of T_C^ρ moving to high temperature in agreement with the T_C^χ of $\chi(T)$. Additionally, ρ_{ab} reveals a weak upturn below ~ 25 K, where it follows a $-\log(T)$ dependence with decreasing temperature suggesting a 2D weak localization behavior. On compressing further to 7.0 GPa, T_C^ρ surges rapidly to 193 K consistent with $\chi(T)$ data. At the same time, $-\log(T)$ upturn in ρ_{ab} is gradually suppressed uncovering a metallic state. At high pressure, precise determination of T_C^ρ becomes difficult due to the broad anomaly, yet signature of $T_C^\rho \sim 250$ K can be traced up to 9.1 GPa.

At 7.0 GPa, ρ_{ab} follows a power-law, $\rho_{ab} = \rho_0 + AT^n$ with an exponent $n \sim 1.9$ below $T_{FL} \sim 14$ K, a hallmark of Fermi-liquid (FL) state. It is worthy to note that at this pressure, ρ_{ab} is higher than the Mott-Ioffe-Regel limit of resistivity defined as $\rho_M^{2D} \cong 0.055(c/a_0) \sim 0.6 \text{ m}\Omega \text{ cm}$, where c is the average separation between CrGeTe₃ layers and $a_0 = 0.529 \text{ \AA}$ is the Bohr radius [44].

Aside, the residual resistivity ratio (RRR), $\rho_{300\text{K}}/\rho_{2\text{K}} \simeq 2$ clearly indicates a bad metal behavior. The RRR and temperature window, where $\rho_{ab} < \rho_M^{2\text{D}}$, increases with rising pressure. Simultaneously, T_{FL} grows to 56 K at 11.0 GPa [Fig.3(c)] and A -coefficient of T^2 -term drops by more than two orders of magnitude, a clear indication of widening of the FL region at higher pressure with decreasing correlation strength.

To obtain more insight about this metallic state, we measured inter-layer resistivity, ρ_c , of another piece of single crystal from the same batch as shown in Fig.3(d). Unlike ρ_{ab} , ρ_c continue to be semiconducting down to the lowest temperature at 6.0 GPa. Intriguingly, ρ_c is nearly temperature independent deep inside the metallic state even at 10.0 GPa, conveying an incoherent inter-layer charge transport and confinement of charge carriers in the ab -plane. This becomes increasingly clear from the temperature dependence of resistivity anisotropy, ρ_c/ρ_{ab} as in shown Fig.3(e). For $P < 5.0$ GPa, $\rho_c/\rho_{ab} \simeq 10^3$ - 10^4 , whereas ρ_c/ρ_{ab} reaches as high as $\sim 10^5$ at 10.0 GPa and 2 K. Such a large value of ρ_c/ρ_{ab} is comparable with that of several strongly correlated materials like high- T_c cuprates [45], manganites [46] and organic compounds [47]. Thus, the pressure induced metallic state in CrGeTe₃ can be regarded as an ideal 2D correlated Fermi metal.

The P - T phase diagram [Fig.4(a)], constructed from susceptibility and resistivity data, unveils a fascinating evolution of the electronic and magnetic properties of CrGeTe₃ when pressure is continuously varied. With adjustment of pressure, CrGeTe₃ alter from an insulator with $T_C \sim 66$ K at ambient pressure to a FMM with T_C surpassing 250 K. The moderate decrease of T_C to ~ 54 K as pressure is raised to 4.5 GPa and subsequent dramatic four-fold rise of T_C in a rather narrow pressure range $4.5 \leq P \leq 6.5$ GPa emphasizes the competition between FMI and FMM phase. The phase diagram also unearth a correlated 2D Fermi metal for $P \geq 7.0$ GPa, significantly well below the 2D to 3D structural phase transition pressure ~ 18 GPa [39], revealing a contrasting feature of CrGeTe₃ with the CrSiTe₃ [38] and isostructural MPX_3 ($M = \text{V, Fe, Mn, Ni}$ and $X = \text{S, Se}$) compounds.

When pressurized, MPX_3 undergo an IMT accompanied by an iso-symmetric structural transition, forming a M - M dimer due to direct overlap between neighboring t_{2g} orbitals of M ions [48–52]. Therefore, a spin-crossover from high-spin to low-spin state occurs together with a large volume collapse. On the other hand, the non-existence of such lattice change close to IMT of CrGeTe₃ [35, 39], assert that direct interaction between t_{2g} -electrons of neighboring Cr atoms is still weak. In fact, this is compatible with the nearly pressure independence of M_S affirming the survival of localized high spin ($S = 3/2$) state of t_{2g} -manifolds even in high pressure state [Fig.4(b)]. Rather, these observations hint the active $Cr-e_g$ orbital plays major role in stabilizing the high pres-

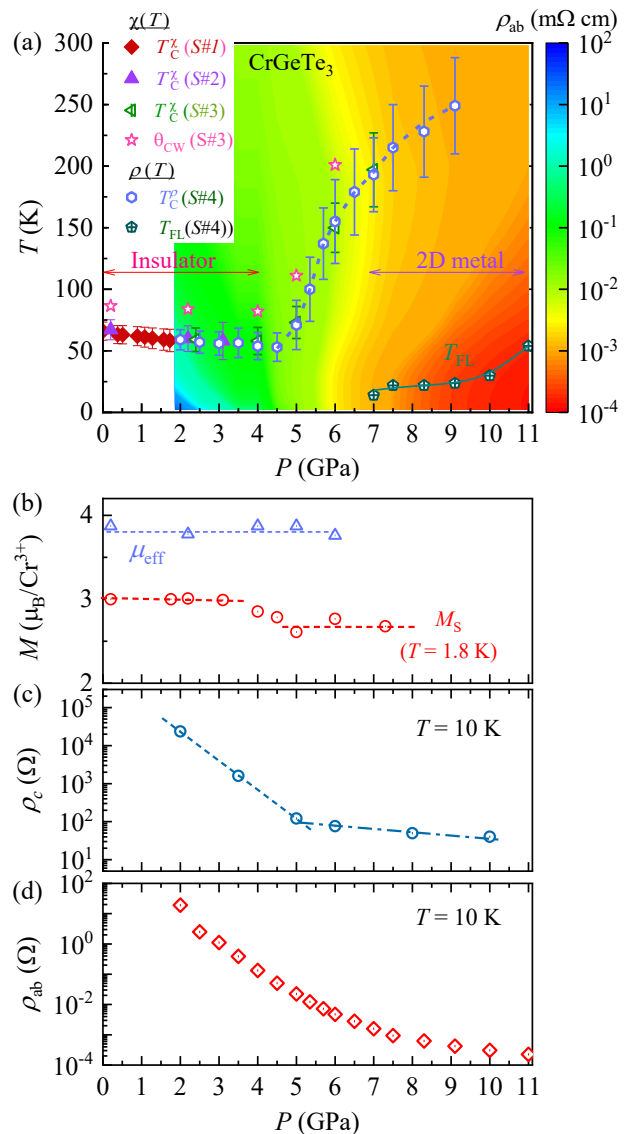


FIG. 4. (a) Pressure temperature phase diagram of CrGeTe₃. Color scale represents the magnitude of ρ_{ab} . θ_{CW} and T_C^{χ} respectively are the Curie-Weiss temperature and Curie temperature, estimated from magnetic susceptibility. T_C^{ρ} and T_{FL} are Curie temperature and Fermi liquid temperature determined from ρ_{ab} . (b) Pressure dependence of effective moment, μ_{eff} , and saturation magnetic moment M_S (at $T = 1.8$ K). (c) and (d) pressure dependence of inter-layer resistivity, ρ_c , and in-plane resistivity ρ_{ab} at $T = 10$ K, respectively.

sure metallic state in CrGeTe₃, thus averting a structural transition as recently proposed for NiPS₃ (Ref.[52]). Moreover, the remarkable absence of concomitant structural distortion across the IMT signify that the pressure induced modification of magnetic and electronic ground states of CrGeTe₃ are purely electronic in origin.

Having discussed the phase diagram, now we qualitatively explain the origin of such intriguing pressure dependent T_C of CrGeTe₃. For a ferromagnet in 2D limit,

the MAE, K , along with the spin-exchange interaction, J , determine $T_C \sim J/\ln(3\pi J/4K)$ [53]. For CrGeTe₃, K ($\simeq -0.05$ meV), usually set by SOC and influence the direction of magnetic easy axis [9, 25], is much smaller in energy scale compared to J ($\simeq 3.0$ meV) [9, 54, 55]. Thus, the strength of exchange interaction plays a major role in fixing the T_C . As explained earlier in Fig.1(c), the FM order in CrGeTe₃ is mainly driven by indirect superexchange interaction, J_{SE} , between Cr- e_g orbitals via two orthogonal Te- p orbitals. With such orbital arrangement, the superexchange integral can be written as [56, 57]

$$J_{SE} \sim -\frac{t_{pd}^2 t_{p'd'}^2 J_H^{\text{Te}}}{\Delta_{CT}^2 (2\Delta_{CT} + U_p)^2}, \quad (1)$$

where $t_{pd}(t_{p'd'})$ is the virtual hopping between $e_g(e'_g)$ and $p(p')$ orbital, J_H^{Te} is the Hund's coupling on Te ion, U_p is the Coulomb interaction on Te site and Δ_{CT} is the charge transfer energy gap between Te- p valence band top and bottom of the Cr- e_g conduction band. Also, J_{SE} depends on the geometrical Cr-Te-Cr bond angle θ . Pressure dependent x-ray diffraction studies reveal that θ deviates marginally from 90° under pressure even up to 10.0 GPa [35, 39, 54] and with such small deviation J_{SE} exchange path remains robust [58]. Assuming J_H^{Te} to be unchanged with pressure, from Eq.(1) it is evident that decrease of Δ_{CT} will have much stronger impact on J_{SE} compared to others, since, Δ_{CT} can be several times larger than t_{pd} and U_p . It is credible to expect Δ_{CT} tends to zero on approaching IMT with varying pressure. Indeed, a recent first principle calculation predicts the collapse of p - d energy gap around 7.0 GPa as a result of shortened Cr-Te bond [54]. Therefore, the sharp rise of T_C for $P \geq 4.5$ GPa can be attributed to the dramatic upsurge of intra-layer J_{SE} resulting from the depreciation of Δ_{CT} with pressure.

The initial decrease of T_C and χ up to 4.5 GPa could be attributed to the following reasons. At ambient condition, apart from J_{SE} , there exists finite AFM exchange interactions between the next nearest neighbor Cr atoms in the layer as well as between the Cr atoms in adjacent layers [9, 24, 54, 55]. With growing pressure these AFM interactions will compete with J_{SE} , as they are expected to strengthen due to shrinking distance between Cr atoms and vdW gaps between adjacent layers. Another is the sign change of K from negative to positive with pressure, that will trigger an alteration of magnetic easy axis from c -axis to ab -plane as reported in pressure dependent magnetoresistance study [36]. However, when pressure exceeds 4.5 GPa, J_{SE} overcomes this competition due to depreciating charge gap with pressure. The distinct pressure dependence of ρ_c and ρ_{ab} , respectively displayed in Fig.4(c) and (d), back up the dominance of intra-layer J_{SE} at high pressure region. Up to 5.0 GPa, ρ_c drops more than two orders of magnitude, whereas it

decreases barely in between 6.0 to 10.0 GPa. By contrast, ρ_{ab} continue to plunge up to 11.0 GPa. As well, the large $\rho_c/\rho_{ab} \sim 10^5$ in high pressure metallic state points that carriers can hop more easily inside the layer rather than across the layers, making the intra-layer J_{SE} significantly stronger than inter-layer interactions.

In summary, we demonstrate that pressure can be used as a suitable parameter to control both magnetic and electrical properties of CrGeTe₃ by tuning the charge transfer energy gap between Te p valence band and Cr e_g conduction band. Moreover, lack of concurrent structural transition and spin-crossover across the IMT makes CrGeTe₃ an unique vdW material and provides a novel example of bandwidth-controlled IMT. Our results also indicate that the electronic properties of CrGeTe₃ can be much more responsively switched compared to other vdW materials, by external tuning parameter such as doping, thin film strain or electrostatic gating.

We acknowledge fruitful discussions with J.-G. Cheng, K. Matsubayashi, M. K. Ray and K. Murata. This work was financially supported by the JSPS KAKENHI Grant numbers JP19H00648 and 19H01836. The work at SNU was supported by grant no. 2019R1A2C2090648, 2019M3E4A1080227 and 2016K1A4A3914691 through the National Research Foundation of Korea funded by the Korean government.

* dilipkbhoi@issp.u-tokyo.ac.jp

- [1] K. S. Burch, D. Mandrus and J.-G. Park, *Nature*, **563**, 47-52 (2018).
- [2] B. Huang, M. A. McGuire, A. F. May, D. Xiao, P. Jarillo-Herrero and X. Xu, *Nat. Mater.*, **19**, 1276 (2020).
- [3] C. Gong and X. Zhang, *Science* **363**, eaav4450 (2019).
- [4] D. Zhong, K. L. Seyler, X. Linpeng, R. Cheng, N. Sivadas, B. Huang, E. Schmidgall, T. Taniguchi, K. Watanabe, M. A. McGuire *et al.*, *Sci. Adv.* **3**, e1603113 (2017).
- [5] X. Yao, B. Gao, M.-G. Han, D. Jain, J. Moon, J. W. Kim, Y. Zhu, S.-W. Cheong and S. Oh, *Nano Lett.*, **19**, 4567 (2019).
- [6] K. L. Seyler, D. Zhong, B. Huang, X. Linpeng, N. P. Wilson, T. Taniguchi, K. Watanabe, W. Yao, D. Xiao, M. A. McGuire, Kai-Mei C. Fu *et al.*, *Nano Lett.*, **18**, 3823 (2018).
- [7] C. Xu, J. Feng, M. Kawamura, Y. Yamaji, Y. Nahas, S. Prokhorenko, Y. Qi, H. Xiang, and L. Bellaiche, *Phys. Rev. Lett.* **124**, 087205 (2020).
- [8] C. Xu, J. Feng, H. Xiang and L. Bellaiche, *npj Comput. Mater.* **4**, 57 (2018).
- [9] C. Gong, L. Li, Z. Li, H. Ji, A. Stern, Y. Xia, T. Cao, W. Bao, C. Wang, Y. Wang *et al.*, *Nature*, **546**, 265 (2017).
- [10] V. Cartheaux, D. Brunet, G. Ouvrard and G. Andre *et al.*, *J. Phys. Condens. Matter*, **7**, 69 (1995).
- [11] M. A. McGuire, H. Dixit, V. R. Cooper and B. C. Sales, *Chem. Mater.* **27**, 612 (2015).
- [12] I. Tsubokawa, *J. Phys. Soc. Japan* **15**, 1664 (1960).
- [13] B. Huang, G. Clark, E. Navarro-Moratalla, D. R. Klein,

- R. Cheng, K. L. Seyler, D. Zhong, E. Schmidgall, M. A. McGuire *et al.*, *Nature*, **546**, 270 (2017).
- [14] Z. Zhang, J. Shang, C. Jiang, A. Rasmita, W. Gao, and T. Yu, *Nano. Lett.* **19**, 3138 (2019).
- [15] H. H. Kim, B. Yang, S. Li, S. Jiang, C. Jin, Z. Tao, G. Nichols, F. Sfigakis, S. Zhong, C. Li, S. Tian *et al.*, *Proc. Natl. Acad. Sci.* **116**, 11131 (2019).
- [16] D. C. Freitas, R. Weht, A. Sulpice, G. Remenyi, P. Strobel, F. Gay, J. Marcus, and M. N.-Regueiro, *J. Phys.: Condens. Matter* **27**, 176002 (2015).
- [17] X. Zhang, Q. Lu, W. Liu, W. Niu, J. Sun, J. Cook, M. Vaninger, P. F. Miceli, D. J. Singh, S.-W. Lian *et al.*, *Nat. Commun.* **12**, 2492 (2021).
- [18] H. J. Deiseroth, K. Aleksandrov, C. Reiner, L. Kienle, and R. K. Kremer, *Eur. J. Inorg. Chem.* **2006**, 1561 (2006).
- [19] B. Chen, J. Yang, H. D. Wang, M. Imai, H. Ohta, C. Michioka, K. Yoshimura, and M. Fang, *J. Phys. Soc. Japan* **82**, 124711 (2013).
- [20] Y. Deng, Y. Yu, Y. Song, J. Zhang, N. Z. Wang, Z. Sun, Y. Yi, Y. Z. Wu, S. Wu, J. Zhu *et al.*, *Nature* **563**, 94 (2018).
- [21] Z. Fei, B. Huang, P. Malinowski, W. Wang, T. Song, J. Sanchez, W. Yao, Di Xiao, X. Zhu, A. F. May *et al.*, *Nat. Mater.* **17**, 778 (2018).
- [22] S. Kang, S. Kang, and J. Yu, *J. Electron. Mater.* **48**, 1441 (2019).
- [23] M. Suzuki, B. Gao, K. Koshiishi, S. Nakata, K. Hagiwara, C. Lin, Y. X. Wan, H. Kumigashira, K. Ono, S. Kang *et al.*, *Phys. Rev. B*, **99**, 161401(R) (2019).
- [24] J. Zhang, X. Cai, W. Xia, A. Liang, J. Huang, C. Wang, L. Yang, H. Yuan, Y. Chen, S. Zhang *et al.*, *Phys. Rev. Lett.* **123**, 047203 (2019).
- [25] D.-H. Kim, K. Kim, K.-T. Ko, J. Seo, J. S. Kim, T.-H. Jang, Y. Kim, J.-Y. Kim, S.-W. Cheong, and J.-H. Park, *Phys. Rev. Lett.* **122**, 207201 (2019).
- [26] M. D. Watson, I. Marković, F. Mazzola, A. Rajan, E. A. Morales, D. M. Burn, T. Hesjedal, G. van der Laan, S. Mukherjee, T. K. Kim *et al.*, *Phys. Rev. B* **101**, 205125 (2020).
- [27] A. K. Kundu, Y. Liu, C. Petrovic, and T. Valla, *Sci. Rep.* **10**, 15602 (2020).
- [28] Z. Wang, T. Zhang, M. Ding, B. Dong, Y. Li, M. Chen, X. Li, J. Huang, H. Wang, X. Zhao *et al.*, *Nat. Nanotechnol.* **13**, 554 (2018).
- [29] S. Jiang, L. Li, Z. Wang, K. F. Mak, and J. Shan, *Nat. Nanotechnol.* **13**, 549-553 (2018).
- [30] I. A. Verzhbitskiy, H. Kurebayashi, H. Cheng, J. Zhou, S. Khan, Y. P. Feng, and G. Eda, *Nat. Electron.*, **3**, 460 (2020).
- [31] N. Wang, H. Tang, M. Shi, H. Zhang, W. Zhuo, D. Liu, F. Meng, L. Ma, J. Ying, L. Zou *et al.*, *J. Am. Chem. Soc.*, **141**, 17166 (2019).
- [32] D. Weber, A. H. Trout, D. W. McComb, and J. E. Goldberger, *Nano Lett.* **19**, 5031 (2019).
- [33] T. Song, Z. Fei, M. Yankowitz, Z. Lin, Q. Jiang, K. Hwangbo, Q. Zhang, B. Sun, T. Taniguchi, K. Watanabe *et al.*, *Nat. Mater.*, **18**, 1298 (2019).
- [34] T. Li, S. Jiang, N. Sivadas, Z. Wang, Y. Xu, D. Weber, J. E. Goldberger, K. Watanabe, T. Taniguchi, C. J. Fennie *et al.*, *Nat. Mater.* **18**, 1303 (2019).
- [35] Y. Sun, R. C. Xiao, G. T. Lin, R. R. Zhang, L. S. Ling, Z. W. Ma, X. Luo, W. J. Lu, Y. P. Sun, and Z. G. Sheng, *Appl. Phys. Lett.*, **112**, 072409 (2018).
- [36] Z. Lin, M. Lohmann, Z. A. Ali, C. Tang, J. Li, W. Xing, J. Zhong, S. Jia, W. Han, S. Coh *et al.*, *Phys. Rev. Mater.* **2**, 051004(R) (2018).
- [37] S. Mondal, M. Kannan, M. Das, L. Govindaraj, R. Singha, B. Satpati, S. Arumugam, and P. Mandal, *Phys. Rev. B* **99**, 180407(R) (2019).
- [38] W. Cai, H. Sun, W. Xia, C. Wu, Y. Liu, H. Liu, Y. Gong, D.-X. Yao, Y. Guo, and M. Wang, *Phys. Rev. B* **102**, 144525 (2020).
- [39] Z. Yu, W. Xia, K. Xu, M. Xu, H. Wang, X. Wang, N. Yu, Z. Zou, J. Zhao, L. Wang, X. Miao, and Y. Guo, *J. Phys. Chem. C*, **123**, 13885 (2019).
- [40] H. Ji, R. A. Stokes, L. D. Alegria, E. C. Blomberg, M. A. Tanatar, A. Reijnders, L. M. Schoop, T. Liang, R. Prozorov, K. S. Burch *et al.*, *J. Appl. Phys.*, **114**, (2013).
- [41] Y. Liu and C. Petrovic, *Phys. Rev. B*, **96**, 054406 (2017).
- [42] W. Liu, Y. Dai, Y.-E. Yang, J. Fan, L. Pi, L. Zhang, and Y. Zhang, *Phys. Rev. B*, **98**, 214420 (2018).
- [43] N. Hiraoka, K. Whiteaker, M. Blankenhorn, Y. Hayashi, R. Oka, H. Takagi, and K. Kitagawa, *J. Phys. Soc. Jpn.* **90**, 074001 (2021).
- [44] O. Gunnarsson, M. Calandra, and J. E. Han, *Rev. Mod. Phys.* **75**, 1085 (2003).
- [45] S. Ono, and Y. Ando, *Phys. C Supercond.*, **388-389**, 321 (2003).
- [46] H. Kuwahara, T. Okuda, Y. Tomioka, A. Asamitsu, and Y. Tokura, *Phys. Rev. Lett.*, **82**, 4316-4319 (1999).
- [47] Y. Shimizu, and R. Kato, *Phys. Rev. B*, **97**, 125107 (2018).
- [48] Y. Wang, Z. Zhou, T. Wen, Y. Zhou, N. Li, F. Han, Y. Xiao, P. Chow, J. Sun, M. Pravica *et al.*, *J. Am. Chem. Soc.*, **138**, 15751 (2016).
- [49] C. R. S. Haines, M. J. Coak, A. R. Wildes, G. I. Lampronti, C. Liu, P. Nahai-Williamson, H. Hamidov, D. Daisenberger, and S. S. Saxena, *Phys. Rev. Lett.*, **121**, 266801 (2018).
- [50] Y. Wang, J. Ying, Z. Zhou, J. Sun, T. Wen, Y. Zhou, N. Li, Q. Zhang, F. Han, Y. Xiao *et al.*, *Nat. Commun.*, **9**, 1914 (2018).
- [51] M. J. Coak, S. Son, D. Daisenberger, H. Hamidov, C. R. S. Haines, P. L. Alireza, A. R. Wildes, C. Liu, S. S. Saxena, and Je-Geun Park, *npj Quantum Mater.*, **4**, 38 (2019).
- [52] H. S. Kim, K. Haule, and D. Vanderbilt, *Phys. Rev. Lett.*, **123**, 236401 (2019).
- [53] Myron Bander and D. L. Mills, *Phys. Rev. B*, **38**, 12015(R) (1988).
- [54] A. O. Fumega, S. Blanco-Canosa, H. Babu-Vasili, P. Gargiani, H. Li, J.-S. Zhou, F. Rivadulla, and V. Pardo, *J. Mater. Chem. C*, **8**, 13582-13589 (2020).
- [55] G. Menichetti, M. Calandra, and M. Polini, *2D Mater.*, **6**, 045042 (2019).
- [56] S. V. Streltsov and D. I. Khomskii, *Phys. Rev. B*, **77**, 064405 (2008).
- [57] D. I. Khomskii, K. I. Kugel, A. O. Sboychakov, and S. V. Streltsov, *J. Exp. Theor. Phys.*, **122**, 484 (2016).
- [58] X. J. Dong, J. Y. You, Z. Zhang, B. Gu, and G. Su, *Phys. Rev. B*, **102**, 144443 (2020).